Optics & Laser Technology 162 (2023) 109240

Contents lists available at ScienceDirect

Optics and Laser Technology

journal homepage: www.elsevier.com/locate/optlastec

Full length article

Femtosecond laser-made 3D micro-chainmail scaffolds towards regenerative medicine

Linas Jonušauskas [a,*], Arnoldas Pautienius [b,c], Eglė Ežerskytė [d], Juozas Grigas [b,c], Deividas Andriukaitis [a], Henrikas Gricius [a], Tomas Baravykas [e], Dovilė Andrijec [e], Rokas Vargalis [e], Greta Bandzevičiūtė [b], Arūnas Stankevičius [b]

[a] Laser Research Center, Vilnius University, Sauletekio Ave. 10, Vilnius, LT-10223, Lithuania
[b] Laboratory of Immunology, Department of Anatomy and Physiology, Faculty of Veterinary Medicine, Lithuanian University of Health Sciences, Tilžės str. 18, Kaunas, LT-47181, Lithuania
[c] Virology Laboratory, Institute of Microbiology and Virology, Faculty of Veterinary Medicine, Lithuanian University of Health Sciences, Tilžės str. 18, Kaunas, LT-47181, Lithuania
[d] Faculty of Chemistry and Geosciences, Vilnius University, Naugarduko str. 24, Vilnius, LT-03225, Lithuania
[e] Femtika Ltd., Keramiku st. 2, Vilnius, LT-10233, Lithuania

ARTICLE INFO

Keywords:
Femtosecond laser
3D printing
Biofabrication

ABSTRACT

Regenerative medicine is a rapidly developing field with far-reaching potential. To sustain progress in this field, new advanced structures are needed. These include scaffolds for cell growth. Direct laser writing (DLW) based on femtosecond laser multi-photon polymerization (MPP) was shown to be an attractive technology for such structure fabrication as it combines vast selection of materials and the possibility to choose feature size in scaffold to be smaller, bigger, or around the same size as a cell. At the same, there are issues related to throughput which limit the widespread implementation of MPP for scaffold manufacturing. It is further compounded by some material limitations making it difficult to print mechanically flexible scaffolds for soft tissue regeneration. In this paper, we propose printing mechanically flexible scaffolds out of mechanically rigid material SZ2080 by employing chainmail architecture. We explore capabilities to optimize the printing procedure of this kind of scaffold, achieving printing times of less than 10 min for a 1 × 1 mm scaffold while maintaining micro-level precision. The superb biocompatibility of such scaffolds is shown both qualitatively and quantitatively and is proven to be independent of the used photoinitiator. Finally, manipulations of scaffolds with cells are performed with no adverse impact on the cell viability or proliferation after such procedures. Overall, this work proposes a methodology for rapid printing of shape-shifting scaffolds which could be used in regenerative medicine both for cell cultivation and potential direct implantation into soft tissue.

1. Introduction

Multi-photon polymerization (MPP) based direct laser writing (DLW) has become a well-established tool for high-precision additive 3D micro- and nanomanufacturing [1]. Through the years it was demonstrated to be suitable for producing structures for numerous applications, such as photonics [2,3], microoptics [4,5], organs-on-chip [6,7], microfluidics [8,9] and micromechanics [10,11]. There are multiple reasons which led to the wide proliferation of this technique. First off, it allows continuously vary feature size/resolution of produced voxels from hundreds of μm down to hundreds of nm [12], with the option to go to tens of nm if specialized methodologies are applied [13,14]. This then can be leveraged to perform true 3D manufacturing, where the shape of the object is created not only in standard 3D printing layer-by-layer fashion but also by continuously scanning the volume of the material in 3D [15,16]. Additionally, it provides a convenient way of controlling the polymerization degree of produced structures, which then allows to tune the refractive index [17] and mechanical properties [18] of the final prints. The overall selection of materials is also wide [19–21], allowing to choose the material best suited for any given application. Multi-material printing in a single structure is also possible [22,23]. Thus, overall, MPP has many advantages which can be exploited in various highly imaginative ways.

One of the fastest growing areas where MPP is being employed is biomedical research and regenerative medicine/veterinary [24,25].

* Corresponding author.
E-mail address: linas.jonusauskas@ff.vu.lt (L. Jonušauskas).

https://doi.org/10.1016/j.optlastec.2023.109240
Received 11 October 2022; Received in revised form 8 January 2023; Accepted 30 January 2023
Available online 15 February 2023

The primary structure used for research in these fields are scaffolds for cell growth [26]. Numerous technologies have been used for this task through the years [27–31]. However, MPP shows the greatest promise in this area due to the possibility to combine all the already listed advantages of this technology towards purpose-built structures. These include but are not limited to cell investigation [32–34], culturing [35, 36] and scaffolds for tissue engineering [37,38]. The last application is extremely promising, as such scaffolds could potentially offer a way to completely rebuild tissues damaged or destroyed by severe injury or disease. However, while current progress in the area already reached the pre-clinical stage [38], there are a lot of barriers that limit further advances. One of them is the mechanical and biological properties of the materials used. Indeed, most tissues in the human body are to some extent soft, while the most common pre-polymers applied in MPP are hard [18,39–41]. Logically, it means that scaffolds made out of such materials can only be used for hard tissues in the body, such as bone. Otherwise, the rigidity of scaffolds might become counterproductive, creating inflammation points, or even breaking after implantation subsequently creating multiple micro-shards which could cause multiple problems. To combat this various biomaterials are being investigated [42–46], but in a lot of cases their fabrication properties, such as ease of printing or mechanical stability leave a lot to be desired. Soft materials are also being proposed, but a lot of them are non-ideal either due to an excessive (more than 10%) shrinkage [47] or poor fabrication properties [48]. This problem is further compounded by the necessity to produce scaffolds in the size range of mm to cm, which requires that materials would permit very high printing speeds and would be mechanically stable enough not to break during the hours-long manufacturing process. This rules out thermal polymerization *via* ultrashort pulse exposure, as it requires substantial overlap of laser pulses resulting in necessity to limit translation velocity (v) to just few mm/s [49]. Therefore, there is a capability gap in MPP for producing scaffolds suitable for soft tissue regeneration.

To combat this challenge, unconventional thinking is required with regards to MPP capabilities. While soft tissues seemingly would require scaffolds made out of soft materials, the alternative would be to just produce a shape-shifting scaffold out of well-known rigid pre-polymer. Here we have to remember that MPP allows assembly-free movable 3D structure printing [11,12,50]. This allows us to look into the hard nature of most pre-polymers not as a limitation, but as an advantage, allowing us to produce scaffolds that could move independently of material properties. One option to achieve viable movable scaffolds out of rigid materials would be producing numerous very small sub-structures that then can be seeded with cells and used as a paste [51,52]. In that case, parts of the final scaffold are ‘‘assembled’’ during the delivery of the paste to the tissue defect. Nevertheless, such an option requires multiple mixing steps before usage, and quite a specific post-development manipulation of produced structures before cell seeding resulting in difficulties with real-world implementation and widespread application. Therefore, in this work, we investigate the possibility to produce shape-shifting chainmail scaffolds [53] for regenerative medicine out of very popular hard pre-polymer SZ2080 [54]. Then, such ring structure can be printed as single-layer chainmail but later put in the irregular shaped wound or damaged tissue and conform to that shape, forming 3D scaffold structure in it for cell growth. Such structure also does not need to be biodegradable, as it acts as micro-level equivalent of medical stitches. Also, data comparing advantages of biodegradable and non-biodegradable scaffolding for cell growth is scarce, use of non-biodegradable polymer scaffolding has previously been tested and ensured effective cell proliferation [55]. Inert and biocompatible non-biodegradable scaffold would provide a long-term attachment point for cells and tissue regeneration, eliminating the need for multiple interventions in cases where scaffold degrades prematurely. We propose and test an advanced printing strategy, which enables using linear printing with v of 10 cm/s. It allows to produce mm-sized scaffolds in a matter of minutes. Furthermore, we qualitatively and quantitatively show that such movable rings are superb for cell proliferation and growth. Overall, the presented results allow us to consider ring or other similar intertwined element-based shape-shifting scaffolds made out of hard material as an attractive alternative to similar structures made out of soft polymer.

2. Materials & methods

2.1. Materials

A standard pre-polymer SZ2080 was used for the work [54]. It was chosen as it has nominal shrinkage [54], well characterized mechanical properties [18], allows usage of cm/s level v [12], and has an overall wide fabrication window [46]. Two variations then were produced using different photoinitiators: with 1 wt% of photoinitiator Irgacure 369 (IRG) and 0.5 wt% 4,4’-bis(dimethylamino)benzophenone (BIS). The idea behind testing and comparing them in this work is severalfold. First, SZ2080 with both of these photoinitiators can be easily tested with our setup, while in some cases one or the other needs to be chosen due to their absorption peculiarities [56]. Also, knowledge about any other differences between scaffolds made out of these two SZ2080 variations would be useful. Pre-polymer was prepared for structuring by drop-casting material on the glass substrate. They were pre-backed at 60 °C for 2 h to turn liquid resin into a hard gel. Development was carried out in 4-methylpentan-2-one for 45 min.

2.2. Laser fabrication setups

Fabrication was performed using ‘‘Laser Nanofactory’’ setup [12] tuned for polymerization [Fig. 1]. The main laser is Erbium-based fiber femtosecond (fs) oscillator ‘‘C-Fiber 780’’ (Menlo Systems GmbH) outputting ~780 nm fundamental wavelength, at 100 MHz repetition rate and 100 fs pulse duration. The oscillator was chosen for this setup because due to the very high repetition rate it is better suited for high-speed printing than kHz-level amplified fs-laser systems which start to show limitations due to decreasing pulse overlap during structuring [15]. As it was shown in the literature [57], even at these repetition rates, there should be virtually no thermal accumulation when nonlinear polymerization optimized material is used and pulse duration does not exceed ~100 fs. Process might become more complex if longer pulses in the range of hundreds of fs and/or material without photo-sensitizing are used [58]. Therefore, we consider that polymerization process presented in this work is based on nonlinear absorption and not thermal polymerization. The laser radiation is directed to the beam control unit (BCU) which houses acousto-optical elements acting as power control elements and fast shutter, as well as dispersion compensation optics, which guarantees that the pulse duration before the objective is ~100 fs.

2.3. Biocompatibility testing

Cell lines tested for capacity to populate the scaffold were immortalized rat liver (WB-F344 Cellosaurus Accession No. CVCL-9806) and monkey kidney (Vero ATCC No. CCL-81; MARC-145 ATCC No. CRL-12231) cells. All cells were cultured in maintenance medium consisting of Minimum Essential Medium (MEM; Gibco, Grand Island, NY, USA) with additional 10% heat-inactivated fetal bovine serum (FBS; Gibco, Grand Island, NY, USA), 100 U/ml penicillin and 100 μg/ml streptomycin. Cells were incubated at 37 °C in 5% CO_2 atmosphere.

Laser made scaffolds were disinfected and seeded by a three-step process. Primary disinfection was done by submerging chainmails in 96% ethanol for 5 min. Subsequent washing was done in phosphate-buffered saline (PBS; 1x, pH 7.2; Gibco) with 100U/ml penicillin and 100 μg/ml streptomycin. Finally, cleaned scaffolds were transferred to the chosen cell culture which was in the 96-well large growth area and secure handling tissue culture test plates.

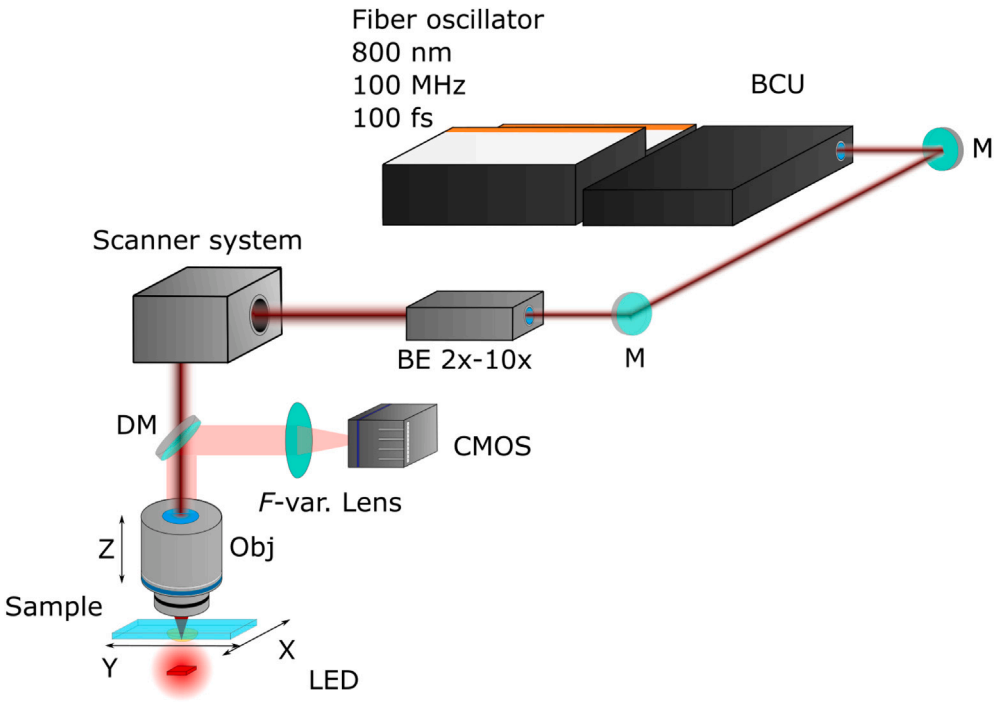

Fig. 1. Schematics of setup used in this work. Here BCU — beam control unit, M - mirrors, BE — automated beam expander, DM — dichroic mirror, F-var — a lens with automated focal distance control, Obj — objective.

Experiment design was as follows: test scaffolds were submerged into maintenance medium in 96-well culture plate containing WB-F344, Vero and MARC-145 cells and incubated alongside control wells for 5 days. All wells were incubated in decuplicates. Test scaffolds were either treated with 0.25% Trypsin-EDTA (Gibco, Grand Island, NY, USA) and harvested for cell counting, or transferred to cell culture wells containing fresh maintenance medium and incubated for additional 5 days before Trypsin-EDTA treatment for a total of 10 days. Cell counting was performed using bright line Neubauer hemocytometer (Thermo Fisher Scientific, Waltham, MA, USA). Optical microscopy images were acquired at days 2 and 10 of cell incubation. Average viable cell count for each cell population was determined by excluding uncharacteristic cells based on forward (FSC) and side scatter (SSC) profiles provided by FACS analysis. Flow cytometry data was analyzed using FlowJo v10 (BD, Franklin Lakes, NJ, USA). Acquired statistical bio-testing results were shown graphically in the form of a boxplot with notches. The notches are defined as $\pm 1.58\mathrm{IQR}/\sqrt{n}$, where IQR is interquartile range and n is number of data points. It represent the 95% confidence interval for each median. Non-overlapping notches give approximately 95% confidence that two medians statistically differ. Differences in results were additionally assessed by Tukey's Honest Significance Test.

3. Results

3.1. Efficient printing of micro-chainmail

Through the years it was shown that MPP technology is the most potent when object size does not exceed several hundred μm. This is due to the fact that most high NA (0.6 and up) objectives have working fields below 500 μ m × 500 μm. As a result, if a structure is around the same size or smaller, it can be easily printed using only galvo-scanners. However, if the size of the structure exceeds the working field of an objective, stitching has to be used [59–61]. This induces optical and mechanical defects to the structure. To overcome this, a synchronization of linear stages and galvo-scanners can be employed [15]. Thus, intuitively, it would seem that for bioscaffold, which needs to be at least $\sim^2$ in overall size, this would be a more suitable option. However, the proposed chainmail structure has some distinct features which might not be ideal for synchronized fabrication. First, the size of rings in this work is 60 μm in diameter, meaning that each ring is smaller than the working field even for high numerical aperture (NA) optics. For instance, the working field of the 0.8 NA objective lens used in this work can be considered 300 μm × 300 μm square, which is 5 times smaller. Also, if the chainmail structure is prepared as a single 3D file, after the slicing step there are huge gaps between rings that have to be traveled by positioning systems between fabricating the rings themselves. Let us take a simple 10 × 10 ring array as an example. 0.8 NA objective, standard $v = 1$ cm/s with slicing step of 1 μm and hatching step of 0.2 μm will be used for calculation. We will choose ring diameter as 60 μm, with ring thickness of 5 μm as such dimensions are relatively similar to the average size of cells. If simple raster scanning with no optimization is used, fabrication time for an array is 29:42 min. [Fig. 2(a)]. Optimization using traveling salesman algorithm [62] can help to reduce overall fabrication time to 7:23 min. [Fig. 2(b)]. Nevertheless, there are still a lot of movements in each overall layer between rings.

The final option of producing rings is one-by-one. Then, the traveling between rings is minimized and the fabrication time of the same 10 × 10 array is 8:17 min. [Fig. 2(c)], i.e. ~3.6 times faster than non-optimized raster fabrication and, surprisingly, 1.1 times slower than optimized single 3D model case. This is due to the fact, that even while fabricating each ring separately, there is a substantial amount of redundant movement inside the ring itself. It is not needed when traveling is done from the ring to ring in the same layer in an optimized case. Take note that in a separate ring fabrication case each ring is fabricated as three parts strategically separated in the Z direction. It is needed, so produced ring is not shadowing the ring being produced next [63,64]. This is also one of the reasons why rings are produced as slanted rings. It also helps to maintain ring diameter even ring-to-ring, because if some rings would be vertical and some horizontal voxel anisotropy [12] would make their shapes irregular. The decision to produce these structures in a layer-by-layer fashion is also deliberate. In standard MPP systems scanners support only X and Y axis, while Z

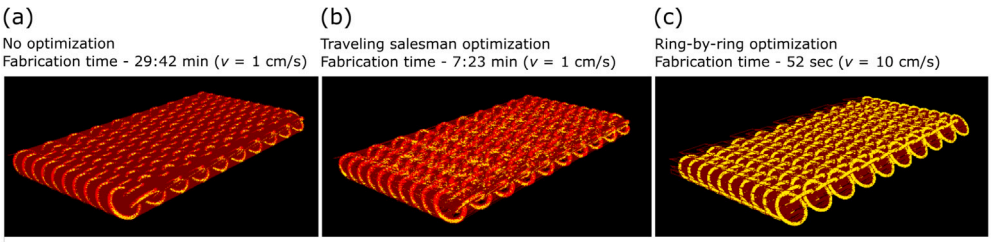

Fig. 2. (a), (b), and (c) show 10 × 10 chainmail array complied for fabrication in a non-optimized single 3D model case, optimized single 3D model method, and ring-by-ring fashion respectively. Yellow lines show laser translations with an open shutter, red — with closed. Structure is only produced during yellow movements, while red jogging just moves from one part of the structure to the other. Thus, reduction of redundant red movements is one of the ways to shorten overall translation trajectory and increase throughput. Note the substantial decrease of red lines as optimization becomes increasingly efficient. This is reflected by fabrication times — 29:42 min for (a), 7:23 min for (b) and 52 s in case of (c). This increase throughput is possible due to shortening of translations within rings, allowing to employ only galvo-scanners and allowing to increase υ 10 fold from 1 cm/s in (a) and (b) to 10 cm/s in (c).

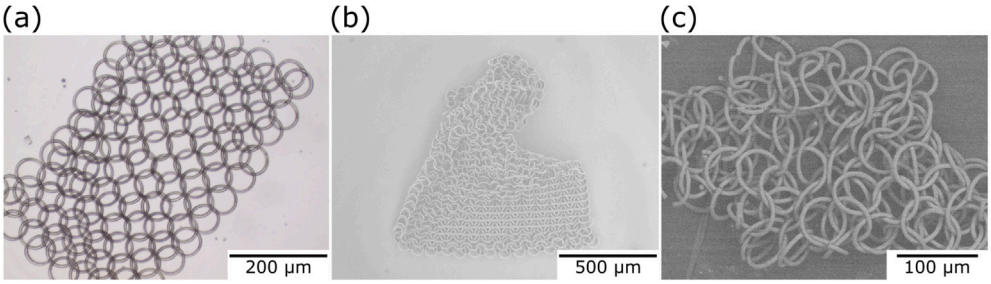

Fig. 3. (a) Optical microscope image of chainmail being released. (b) - SEM micrograph showing partially folded structure. (c) - chainmail after manipulation resulting in complete twisting of the structure. While some rings are broken, overall structural integrity is unaffected and rings are holding together.

is still mechanical, meaning that usage of fast movement is only truly effective for XY axes. Meanwhile, the Z axis has limited applicability in fast 3D scanning. Therefore, true 3D translation was only employed when the movement of the Z-axis is relatively slower than movement in XY, for instance in micro-lens production [15]. Regardless, ring-by-ring fabrication in a layer-by-layer fashion, while not as fast when the same υ is used for the whole array case, allows for the use of only the scanners for ring fabrication. This, in turn, enables to increase υ from standard 1 cm/s to 10 cm/s during ring printing without any loss of structure quality. Surface roughness did not change after this increase as well and was in the range of several hundred nm, as dictated by the "stepping" in the rings due to the layer-by-layer manufacturing method and determined from SEM images. This is acceptable as some surface roughness is desirable for good cell adhesion and growth [65]. Linear stages then move between the rings at υ = 1 cm/s. A similar increase in υ would not be realistic with fully synchronized linear stages and galvo-scanners because feedback timing of synchronized systems (48 kHz or ~20 µs in this system [15]) would lead to linear stages starting to deviate too much before scanners could correct for it. As a result, using such a smart scanning strategy of printing in a ring-by-ring fashion manufacturing time of a 10 × 10 ring array is reduced to ~1 min at υ = 10 cm/s. It is important to note that subsequent tuning of the setup itself or application of inherently faster scanning methodologies [66] could lead to an even higher throughput increase in the future.

After optimization, chainmail printing followed. For bio testing, two main kinds of scaffolds were prepared: 500 × 500 µm for initial testing (10 × 20 rings) and general viability study and 1 × 1 mm ring arrays (20 × 40 rings) for main statistical measurements. The necessity to use a 1:2 aspect ratio for ring amount to acquire square scaffolds was a result of how rings were arranged in a 3D model. υ = 10 cm/s was employed, allowing to produce both kinds of structures in several minutes (~2 min for the small one and ~8 min for the bigger one). Rings were made inside the volume of SZ2080 without securing them to the substrate, allowing them to be release easily during development [Fig. 3(a)]. Subsequent SEM analysis showed that the structures had a good mechanical quality and rings could move easily [Fig. 3(b)–(c)]. Using such protocol 20 + 40 chainmail structures were produced for biotesting 10 + 20 with BIS photoinitiator and 10 + 20 with IRG, where the first number shows the amount of smaller scaffolds and second — main batch numbers. Overall printing time was just over 6 h. This level of throughput provides a capability for MPP to be used for relatively fast on-demand biotesting with a statistically significant amount of scaffolds.

3.2. Biocompatibility testing

The influence of photoinitiator on the biocompatibility of 3D printed structures is argued in the literature quite extensively [46,67–69]. Therefore, a direct comparison between two easily obtainable commercial photoinitiators IRG and BIS was performed as the first bio experiment of this work. Indeed, it is known from literature that even small amounts of these photoinitiators (down to hundreds of µg/L) can be considered toxic [70]. Amount of photoinitiators present in materials before polymerization is in the range of ~%. Therefore, such materials should be inherently toxic. For this testing, chainmails were seeded with cells with minimal manipulation and cell count for all tested cell types (WB-F344, VERO, and MARC-145) was measured. Measurement showed high biocompatibility of all materials to all tested cell lines. For both IRG and BIS photosensitized scaffolds cell growth was very good and almost indistinguishable [Fig. 4]. This can be explained by several factors. First, for scaffold fabrication, we used laser power close to the upper limit of the fabrication window (20 mW for fabrication while the damage threshold was ~22 mW). Therefore, we consider that the polymerization degree of the material was very high [17]. This meant that most of the photoinitiator was used up during the printing process. Also, the rigid polymer matrix of SZ2080 should have prevented left-over photoinitiator molecules from being released [71]. This is in sharp contrast to most hydrogel materials, which tend to swell extensively in different media [22], releasing any leftover monomers and photoinitiators into the environment. Overall, due to this result from this point onwards, we will not differentiate between IRG and BIS

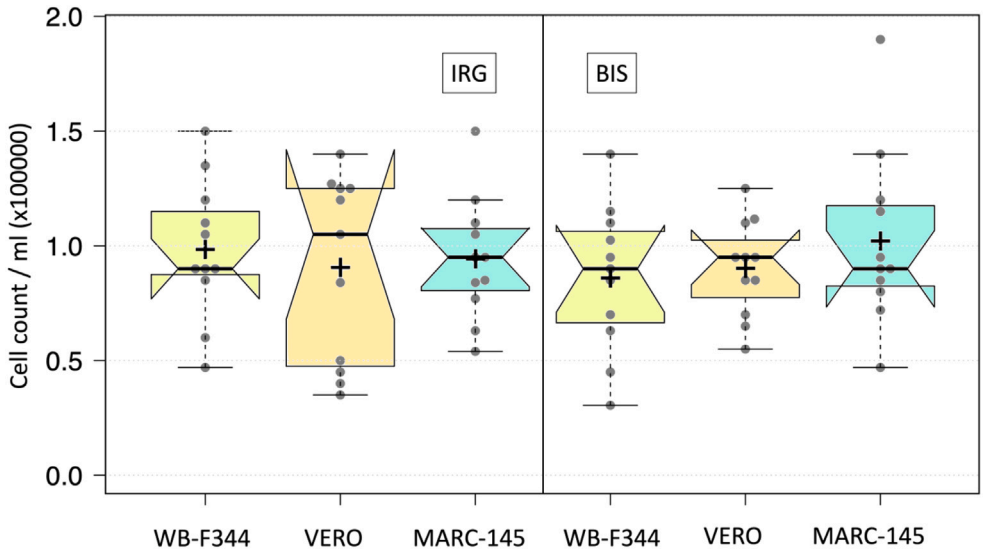

Fig. 4. WB344, VERO, and MARC-145 cell count grown on scaffold affected by different IRG and BIS in SZ2080. Good biocompatibility with no clear difference between tested materials can be observed.

photosensitized SZ2080 when testing cell proliferation and viability. Additionally, it means that if the printing setup is limiting usage of either IRG or BIS due to the spectral reasons of the light source resulting in low two-photon absorption cross-section [46], choosing either of photoinitiators would not impede bio experiments.

The next thing to consider is the manipulation of micro-chainmail. Intuitively, it would seem that after such a structure is developed and released it should be relatively fragile. Indeed, mechanical stability of material should not be overlooked and was studied quite a lot recently, both in stand-alone fashion [18,72] as well as in biological settings [38, 46]. In all of those experiments SZ2080 was shown to be mechanically stable and not prone to breaking, with Young's modulus in the range of 1 GPa (exact value depends on the fabrication parameters) [18]. What we discovered during experimentation is that chainmails made out of SZ2080 photosensitized with IRG were highly resilient to mechanical stress [Fig. 5(a)]. This coincides well with previous works where it was shown to be highly resilient to external stress and usable even for micro-spring manufacturing [12]. However, chainmails made out of SZ2080 photosensitized with BIS showed a tendency to break if manipulated not carefully [Fig. 5(b)]. Explanation for such behavior most likely lies in the relatively more rigid nature of SZ2080 with BIS, which leads to the tendency of structure breaking under mechanical stress. Therefore, SZ2080 scaffolds with BIS required somewhat more gentle manipulation to avoid such mechanical damage.

In order to test both kinds of scaffolds with no mechanical damage occurring special handling protocol was developed. Each scaffold produced was placed in an alcohol filled Eppendorf tube. Before submerging scaffold into a maintenance medium, the alcohol was carefully removed by pipetting the scaffold with PBS. Standard 100–1000 μL tips were utilized for pipetting, however, they were cut shorter to allow the lumen to suit the size of the scaffold without compromising its integrity. Overall this allowed us to perform cell cultivation experiments with very high repeatability without breaking printed structures. Using an optical microscope it was established that all used cell types tend to grow on scaffolds well, in most cases completely covering them [Fig. 6]. These photos show that due to the chosen ring size and configuration cells were growing in free-form manner on all surfaces of the rings, signifying that such structure acts as a true 3D scaffold. What is more, scaffolds were so resilient that after biocompatibility experiments some of them were cleared of cells and new ones were seeded. Cell growth on chainmails during this second time usage was indistinguishable from the first time they were seeded on the scaffolds. While these results were not used for any statistical analysis presented in this work, generally speaking, chainmails (and, potentially, other types of SZ2080-based movable scaffolds) can actually even be considered for multi-time use if cell cultivation is the ultimate goal of the procedure.

Additionally, cell proliferation on scaffolds exceeded what was achieved on flat control samples for all cell types, with WB-F344 cell line having the highest result at ~30% [Fig. 7(a)]. This once again shows how important surface topography is for cell-based experiments [65]. For comparison, when flat SZ2080 with IRG samples were tested against flat glass control, SZ2080 performed relatively worse [46]. One important thing to note is that such ring structure surfaces are, at a micro level, quite rough. Due to the sliced fabrication nature, stepping occurs on the surface, resulting in the surface roughness of a few hundred nm. Exact value is hard to estimate due to roughens varying depending on the ring surface orientation in relation to the slicing direction. Nevertheless, what is important in the biological context, is that such stepping increases effective surface area and allows better adhesion of cells to chains. This hypothesis is supported by the fact that chainmails could be transferred from test plate wells where initial cultivation took place to new ones and cell proliferation would continue. Both cell count and cell viability are rate exceeded 70% in all tested cell types after such an operation [Fig. 8]. Cell count increase after the transfer was up to 28% higher than proliferation on the initial sample for WB-F344 cells and around the same for other cell types [Fig. 7(b)]. This is an very important discovery because such transfer with cells on scaffold would take place during regenerative medicine procedure, where scaffolds with cells would be implanted in the patient's body. Also, our experiments show that the movement of rings during transfer does not influence cells in any adverse way. Thus, even if such a scaffold is produced out of non-biodegradable material, it should not have any negative impact on the patient even though such hard rings would move in relation to each other. At the same time, although the prospect of chainmail use as a scaffold for cell growth in regenerative medicine is far-reaching, several questions remain unaddressed. The immune response plays a significant role in tissue regeneration [73]. Therefore, the interplay between reactions associated with the immune response at the lesion site and the scaffold graft must be investigated. Moreover, as with other forms of inorganic grafting, immunocompatibility between the immune system of the recipient and the scaffold material is crucial for the successful application of chainmail graft technology in regenerative medicine.

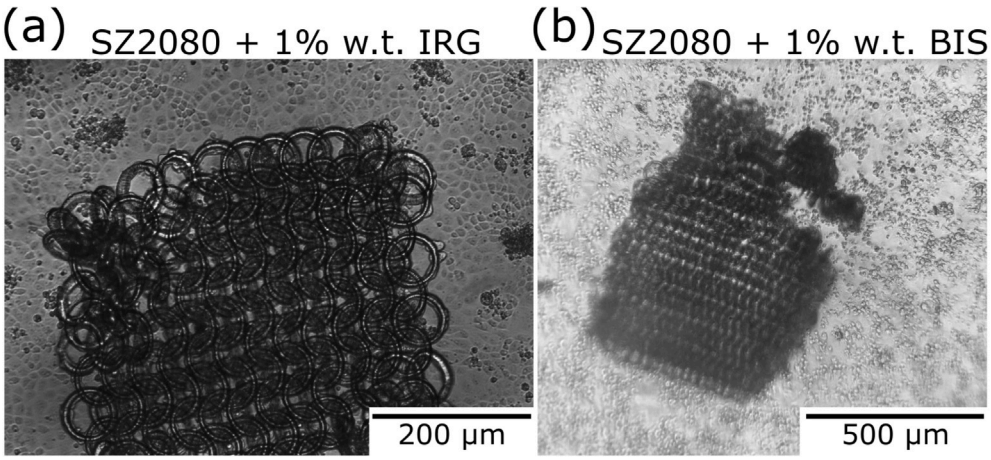

Fig. 5. Difference between mechanical stability of IRG (a) and BIS-based (b) SZ2080 scaffolds during ell seeding and manipulation experiments. IRG containings scaffolds were shown to be substantially more resilient. As a result, a more gentle manipulation protocol was developed.

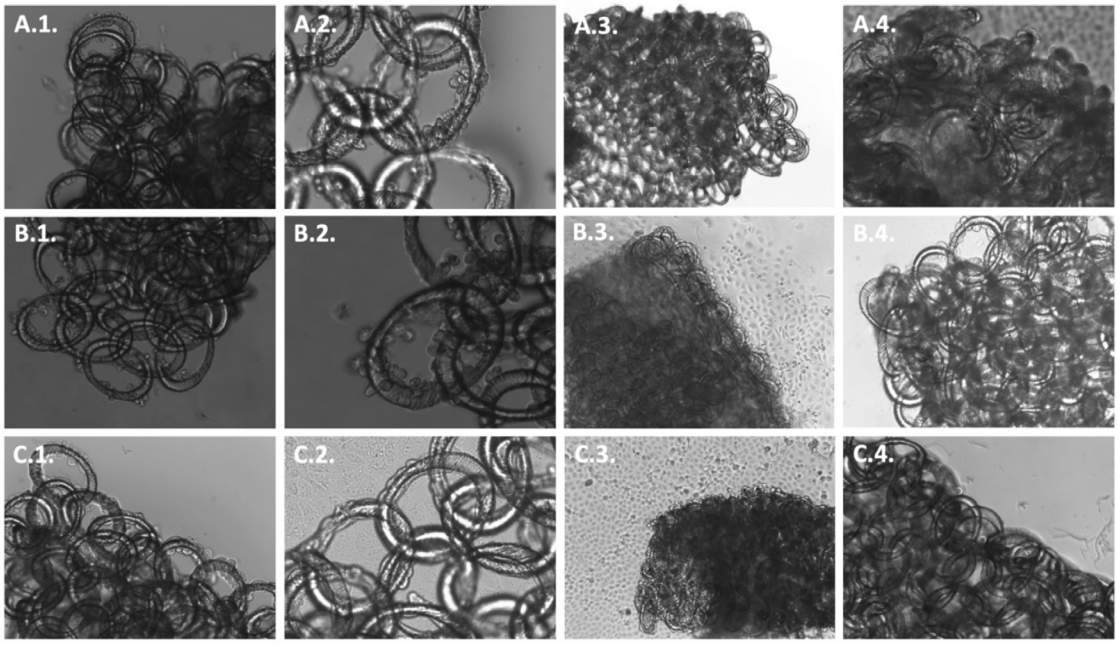

Fig. 6. Optical image of cells growing on the structure. WB-F344 (A), VERO (B), MARC-145 (C) cell lines. Cells after 2 days of cultivation (1,2); after transfer of cell-containing scaffold to cell-free medium at 10-day incubation (3,4). Size reference — all rings are 60 μm in diameter.

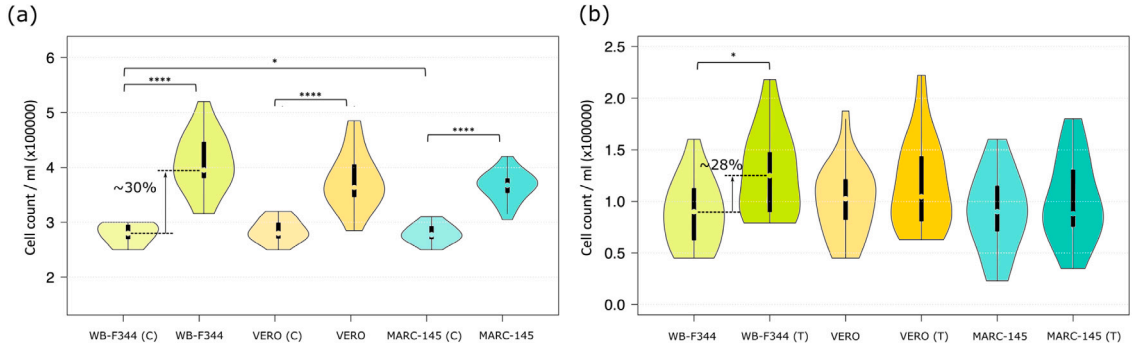

Fig. 7. (a) - WB-F344, VERO, and MARC-145 cell count in the test group that represents overall cell number collected from both scaffold and tissue culture test plate. Control group (C) representing cell number collected from tissue culture test plate after 5-day incubation (* $p < 0.05$; **** $p < 0.0001$). All cell types showed better proliferation on chainmails, with WB-F344 showing the best result with ~30% higher cell count than a control. (b) - Same cell type count change after transfer of cell-containing scaffold to cell-free medium (T) at 10-day incubation (* $p < 0.05$). WB-F344 again showed the best result with proliferation on transferred sample exceeding original by ~28%. Other cell types showed no significant difference between transferred and non-transferred case.

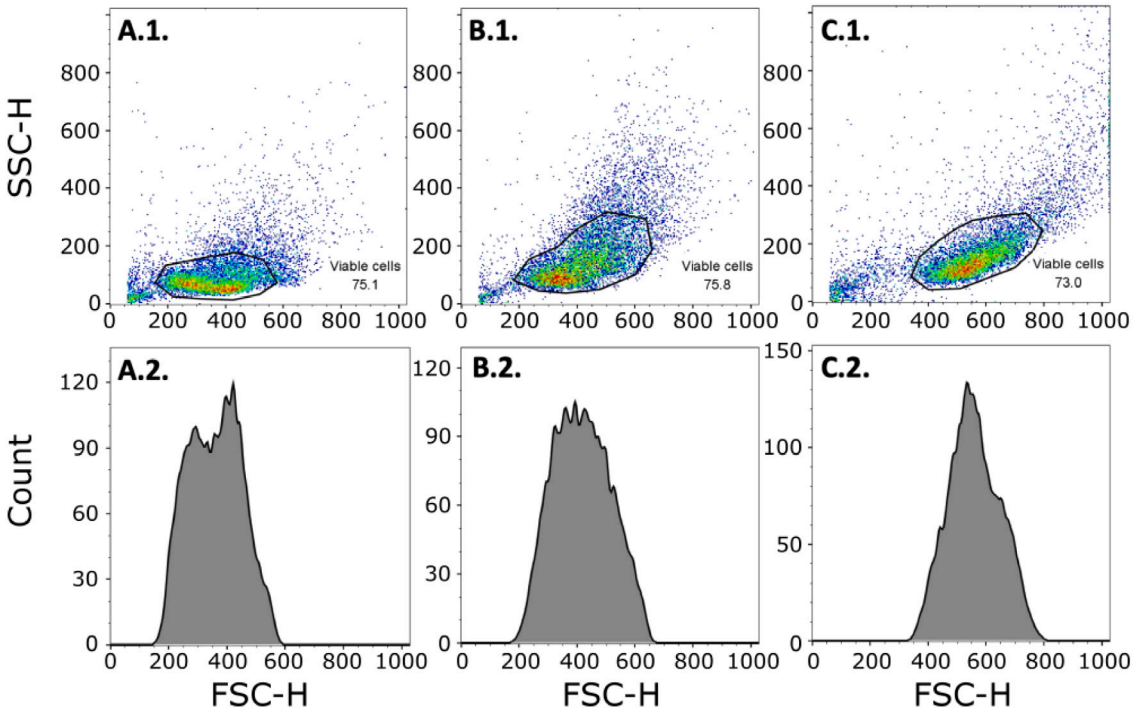

Fig. 8. The average proportion of viable cells in WB344 (A), VERO (B), and MARC-145 (C) cell samples are based on forward (FSC) and side scatters (SSC) profiles. Viable cell gates were established (1) and cell count based on cell size was demonstrated (2). The result is identical to what was to be expected from a standard control experiment, showing that scaffold transfer from one test plate well to other has no negative impact on cell viability.

4. Discussion

Throughput was always considered to be one of the weak points of MPP technology. Fabrication using very small voxels, with a single voxel volume potentially down to less than ~1 μm^3, it is hard to imagine how mm and cm scale structures could be produced in a reasonable time of several h per structure. One way would be to use lower NA, which increases voxel volume [12,74]. However, then one of the main selling points of MPP, its resolution, is lost. Another rather trivial way to increase throughput would be to continuously increase v. Technically it is possible with more and more advanced scanning systems or even by using acousto optical deflectors [66]. Indeed, as of today, there are works claiming of using even $v \geq$ m/s, albeit with NA below 0.5 [75,76]. While this path seems promising, it has a very hard ceiling dictated by the fs laser repetition rate and a gap formed between exposed areas [15]. If an amplified fs laser source is used, at v = 1 cm/s and 1 MHz repetition rate (which is quite common for commercial systems) distance traveled between pulses is 10 nm. If we consider laser spot size of around $2\omega_0$ = 1 μm it means that each exposure is created after the system moved ~1% of the laser spot. At these experimental conditions, such exposure leads to a continuous line. However, if v = 10 cm/s, as used in this work, we get a distance moved of 100 nm which translates to ~10% of the laser spot. This would still be acceptable for continuous lines, but with very little room for further increase in v. There are also questions about how it would impact mechanical properties and if it would make rings break easier. If v would be increased by one more order of magnitude to 100 cm/s = 1 m/s distance between laser exposure would grow to 1 μm, which would mean that no continuous line was formed. The situation, of course, is a lot better with optics that do not focus on such a small laser spot, like f-theta lenses used in ablation/surface structuring [77–79]. Then v can be increased even further as $2\omega_0$ < tens of μm. However, for sub-μm level manufacturing, usage of amplified laser systems for m/s level v is rather limited. Then, MPP is reduced to a role of a supporting function in otherwise subtractive manufacturing-centric hybrid fabrication workstation [8,9,80]. Application of oscillators, which prohibit such systems from hybrid additive–subtractive manufacturing, should allow quite high v, as repetition rate in such systems can go as high as 100 MHz. Then, even at v = 100 m/s distance between pulses would be in the 10 nm range. Therefore, while fs oscillators have a substantially higher ceiling for maximum absolute v, it is still not infinite.

All of this leads to the challenge of finding other methods (or their combinations) to increase the throughput of MPP in the long run. One of the most common ways to do it is to use beam-shaping *via* diffractive optical elements (DOE) or spatial light modulators (SLM). Both of these options were explored quite thoroughly and shown to increase throughput by either shaping of voxel/exposed volume into a more desirable shape [81,82] or distribution or forming multiple focal points [83,84]. The disadvantage of the latter approach is a sacrifice of complete free-form geometry of the structure. Distance between each focal point becomes its independent working area. This is completely acceptable for periodic structures like metamaterials, or chainmail shown in this work. However, for bigger, more complex structures this would be a huge disadvantage, leading to potentially undesirable stitching [59–61]. Thus, the approach of single voxel shaping is more attractive for big, irregular 3D structure printing. While both of these options are attractive, they are highly limited by the repetition rate of current commercial SLMs, the vast majority of which operate at 60 Hz, with faster options being mainly in development [85,86]. Finally, to save time during manufacturing advanced AI-based algorithm optimization could be employed [87,88]. While this alone would not make MPP exceedingly fast, it can be easily paired with other discussed approaches, allowing for the compound advantage gained. Nevertheless, while there are multiple approaches how MPP can be made faster, there is no definite answer to where technology could move after ultrafast scanning and multi-focal printing are exploited to their maximum potential.

One of the major considerations when discussing MPP (and other related technology) usage in regenerative medicine is how easy it would be to introduce proposed structures to the workflow of medical procedures. Modern medical procedures are very complex and require the usage of a lot of different devices, tools, and techniques, which have

to work together in perfect, synergistic harmony. Anything new which would be introduced to medicine with any hope of wide adoption either has to be perceived by medical professionals as compatible with what is already in the use or be so disruptive that there would be enough drive to replace older practices [89,90]. While some literature considers additive manufacturing to be such a revolutionary approach [91–93], the evolutionary approach should not be overlooked. It would lead to fast-track implementation which could start helping patients as soon as possible. Proposed chainmail is more on this side of the spectrum of innovations as created handling protocol uses readily available lab equipment and tools. Additionally, due to being shapeshifting scaffold, it is a lot easier to manipulate, because normally MPP made stiff structures at mm scale, due to very thin features, as shown in this work in the case of BIS containing chainmails, can be relatively fragile. Finally, a procedure for fast printing of such structures could allow printing several square cm sized patches of such chainmail, which then could be cut using standard medical scissors to the size needed for the procedure. In other words, instead of trying to design different scaffolds for each different case of tissue damage, the required size chainmail patch could be cut and then used. As it is a shape-shifting scaffold, it would automatically assume the required shape, without the need for any other complex design procedures. While individualized scaffolds designed for a specific patient and the precise condition is the end goal of additive manufacturing-based regenerative medicine, chainmail allows transitional approach, which, on the one hand should be highly acceptable for medics as it does not require any new tools and procedures to implement, but at the same time would allow to open the door and legitimize additive manufacturing-made scaffolds as a viable and desirable tool in widespread medicine.

Despite the promising results that demonstrate the capacity of immortalized cell adhesion to the surface of the micro-chainmail, the limitations of the study and the future prospects need to be addressed. While our findings confirm the viability of the pre-polymer SZ2080 use for flexible scaffold manufacture and cell binding, more evidence is required to further confirm the capacity of the micro-chainmail as a scaffold for tissue regeneration. Firstly, a wider range of cells, including primary cells, need to be tested. Immortalized cells were selected for this study due to their accessibility, ease of use, and capacity for indefinite replication, which allowed us to establish the time frame required for cells to completely populate the micro-chainmail surface. However, similar experiments should be carried out gradually moving towards the tissue model, starting with individual and combinations of primary cells typically found within the tissue of interest (such as epithelial or connective tissue cells) and eventually attempting to integrate the micro-chainmail graft within an *in vivo* system. Secondly, the host's immune response to any graft is the primary concern of transplantology. We did not test interactions between the structure and immune cells in the present study. However, before its use as a scaffold for tissue regeneration, an extensive investigation of SZ2080 viability as an immunologically inert substance should be carried out.

5. Conclusions

In this work we proposed, produced, and tested micro-chainmail scaffolds for the eventual use in regenerative medicine. Due to the periodic 3D ring array arrangement of such objects, the smart-scanning algorithm was employed using primarily galvo-scanners for laser printing. This allowed us to exploit $v = 10$ cm/s without any adverse impact on the mechanical quality of the rings or loss of micro-level precision. Printing time for one scaffold then was reduced to 2 and 8 min for 500×500 μm and 1×1 mm scaffolds, respectively. Overall, 60 micro-chainmails were produced to assure statistically significant results of biotesting. Overall production time for all 60 scaffolds - ~6 h. SZ2080 pre-polymer was employed for fabrication with two photoinitiators — BIS and IRG, with half of the structures being produced with one and the other half with the second one. Biotesting showed that there is no significant biocompatibility difference between SZ2080 scaffolds with IRG or BIS photoinitiators. However, mechanically, BIS containing chainmails were shown to be somewhat more fragile. To combat this, a special handling procedure was created. To make it more convenient and accessible only standard lab equipment and simple procedures were employed for it. This allowed us to use IRG and BIS-containing chainmails interchangeably. Overall, bio testing showed very high cell proliferation potential on ring-like scaffolds, with cell count on scaffolds exceeding flat control by ~30% after 5 day incubation period. What is more, when the scaffold was transferred from a seeding test plate wells to a new ones, cells continued to proliferate and did it even faster than in the initial growth environment by up to ~28%. Cell viability was also excellent and well within what would be expected from the control. This has serious implications for the field of regenerative medicine, as it offers enabling technology which would enable the simple, fast, cheap, and convenient introduction of MPP-made scaffolds into general medical practices with minimal introduction barriers.

CRediT authorship contribution statement

Linas Jonušauskas: Conceptualization, Methodology, Project administration, Resources, Supervision, Visualization, Writing – original draft. **Arnoldas Pautienius:** Data curation, Formal analysis, Investigation, Methodology, Visualization, Writing – review & editing. **Eglė Eržerskytė:** Data curation, Investigation, Writing – review & editing. **Juozas Grigas:** Data curation, Formal analysis, Investigation. **Deividas Andriukaitis:** Data curation, Investigation, Writing – review & editing. **Henrikas Gricius:** Data curation, Investigation. **Tomas Baravykas:** Software. **Dovilė Andrijec:** Data curation, Investigation, Writing – review & editing. **Rokas Vargalis:** Data curation. **Greta Bandzevičiūtė:** Writing – review & editing. **Arūnas Stankevičius:** Methodology, Project administration, Resources, Supervision, Writing – review & editing.

Declaration of competing interest

The authors declare that they have no known competing financial interests or personal relationships that could have appeared to influence the work reported in this paper.

Data availability

Data will be made available on request.

Funding

This research did not receive any specific grant from funding agencies in the public, commercial, or not-for-profit sectors

References

[1] L. Jonušauskas, S. Juodkazis, M. Malinauskas, Optical 3D printing: bridging the gaps in the mesoscale, J. Opt. 20 (5) (2018) 053001.
[2] M. Deubel, G. Freymann, M. Wegener, S. Pereira, K. Busch, C.M. Soukoulis, Direct laser writing of three-dimensional photonic-crystal templates for telecommunications, Nature Mater. 3 (7) (2004) 444–447, http://dx.doi.org/10.1038/nmat1155.
[3] M. Farsari, A. Ovsianikov, M. Vamvakaki, I. Sakellari, D. Gray, B.N. Chichkov, C. Fotakis, Fabrication of three-dimensional photonic crystal structures containing an active nonlinear optical chromophore, Appl. Phys. A 93 (1) (2008) 11–15, http://dx.doi.org/10.1007/s00339-008-4642-8.
[4] T. Gissibl, S. Thiele, A. Herkommer, H. Giessen, Two-photon direct laser writing of ultracompact multi-lens objectives, Nat. Photonics 10 (8) (2016) 554–560, http://dx.doi.org/10.1038/nphoton.2016.121.
[5] P.-I. Dietrich, M. Blaicher, I. Reuter, M. Billah, T. Hoose, A. Hofmann, C. Caer, R. Dangel, B. Offrein, U. Troppenz, M. Moehrle, W. Freude, C. Koos, In situ 3D nanoprinting of free-form coupling elements for hybrid photonic integration, Nat. Photonics 12 (4) (2018) 241–247, http://dx.doi.org/10.1038/s41566-018-0133-4.

[6] F. Larramendy, S. Yoshida, D. Maier, Z. Fekete, S. Takeuchi, O. Paul, 3D arrays of microcages by two-photon lithography for spatial organization of living cells, Lab Chip 19 (5) (2019) 875–884, http://dx.doi.org/10.1039/c8lc01240g.

[7] L. Bakhchova, L. Jonušauskas, D. Andrijec, M. Kurachkina, T. Baravykas, A. Eremin, U. Steinmann, Femtosecond laser-based integration of nano-membranes into organ-on-a-chip systems, Materials 13 (14) (2020) 3076, http://dx.doi.org/10.3390/ma13143076.

[8] D. Wu, S.-Z. Wu, J. Xu, L.-G. Niu, K. Midorikawa, K. Sugioka, Hybrid femtosecond laser microfabrication to achieve true 3D glass/polymer composite biochips with multiscale features and high performance: the concept of ship-in-a-bottle biochip, Laser Photonics Rev. 8 (3) (2014) 458–467, http://dx.doi.org/10.1002/lpor.201400005.

[9] L. Amato, Y. Gu, N. Bellini, S.M. Eaton, G. Cerullo, R. Osellame, Integrated three-dimensional filter separates nanoscale from microscale elements in a microfluidic chip, Lab Chip 12 (6) (2012) 1135–1142, http://dx.doi.org/10.1039/c2lc21116e.

[10] J. Köhler, S.I. Ksouri, C. Esen, A. Ostendorf, Optical screw-wrench for microassembly, Microsyst. Nanoeng. 3 (1) (2017) http://dx.doi.org/10.1038/micronano.2016.83.

[11] J.C. Williams, H. Chandrahalim, J.S. Suelzer, N.G. Usechak, Two-photon nanomachining of a micromechanically enhanced optical cavity sensor on an optical fiber tip, Adv. Photonics Res. 3 (7) (2022) 2100359, http://dx.doi.org/10.1002/adpr.202100359.

[12] L. Jonušauskas, T. Baravykas, D. Andrijec, T. Gadišauskas, V. Purlys, Stitchless support-free 3D printing of free-form micromechanical structures with feature size on-demand, Sci. Rep. 9 (1) (2019) 17533, http://dx.doi.org/10.1038/s41598-019-54024-1.

[13] R. Wollhofen, J. Katzmann, C. Hrelescu, J. Jacak, T.A. Klar, 120 nm resolution and 55 nm structure size in STED-lithography, Opt. Express 21 (9) (2013) 10831, http://dx.doi.org/10.1364/oe.21.010831.

[14] G. Seniutinas, A. Weber, C. Padeste, I. Sakellari, M. Farsari, C. David, Beyond 100 nm resolution in 3D laser lithography – Post processing solutions, Microelectron. Eng. 191 (2018) 25–31, http://dx.doi.org/10.1016/j.mee.2018.01.018.

[15] L. Jonušauskas, D. Gailevičius, S. Rekštytė, T. Baldacchini, S. Juodkazis, M. Malinauskas, Mesoscale laser 3D printing, Opt. Express 27 (11) (2019) 15205–15221, http://dx.doi.org/10.20944/preprints201810.0384.v1.

[16] S. Hasselmann, L. Hahn, T. Lorson, E. Schätzlein, I. Sébastien, M. Beudert, T. Lühmann, J.C. Neubauer, G. Sextl, R. Luxenhofer, D. Heinrich, Freeform direct laser writing of versatile topological 3D scaffolds enabled by intrinsic support hydrogel, Mater. Horiz. 8 (12) (2021) 3334–3344, http://dx.doi.org/10.1039/d1mh00925g.

[17] A. Žukauskas, I. Matulaitienė, D. Paipulas, G. Niaura, M. Malinauskas, R. Gadonas, Tuning the refractive index in 3D direct laser writing lithography: towards GRIN microoptics, Laser Photonics Rev. 9 (6) (2015) 706–712, http://dx.doi.org/10.1002/lpor.201500170.

[18] L. Pertoldi, V. Zega, C. Comi, R. Osellame, Dynamic mechanical characterization of two-photon-polymerized SZ2080 photoresist, J. Appl. Phys. 128 (17) (2020) 175102, http://dx.doi.org/10.1063/5.0022367.

[19] C. Barner-Kowollik, M. Bastmeyer, E. Blasco, G. Delaittre, P. Müller, B. Richter, M. Wegener, 3D laser micro- and nanoprinting: Challenges for chemistry, Angew. Chem. 56 (50) (2017) 15828–15845, http://dx.doi.org/10.1002/anie.201704695.

[20] M. Carlotti, V. Mattoli, Functional materials for two-photon polymerization in microfabrication, Small 15 (40) (2019) 1902687, http://dx.doi.org/10.1002/smll.201902687.

[21] G. Merkininkaitė, D. Gailevičius, S. Šakirzanovas, L. Jonušauskas, Polymers for regenerative medicine structures made via multiphoton 3D lithography, Int. J. Polym. Sci. 2019 (2019) 1–23, http://dx.doi.org/10.1155/2019/3403548.

[22] S. Rekštytė, D. Paipulas, M. Malinauskas, V. Mizeikis, Microactuation and sensing using reversible deformations of laser-written polymeric structures, Nanotechnology 28 (12) (2017) 124001, http://dx.doi.org/10.1088/1361-6528/aa5d4d.

[23] F. Mayer, S. Richter, J. Westhauser, E. Blasco, C. Barner-Kowollik, M. Wegener, Multimaterial 3D laser microprinting using an integrated microfluidic system, Sci. Adv. 5 (2) (2019) http://dx.doi.org/10.1126/sciadv.aau9160.

[24] C. Mason, P. Dunnill, A brief definition of regenerative medicine, Regen. Med. 3 (1) (2008) 1–5, http://dx.doi.org/10.2217/17460751.3.1.1.

[25] L.A. Dahlgren, Regenerative medicine therapies for equine wound management, Vet. Clin. North Am. 34 (3) (2018) 605–620, http://dx.doi.org/10.1016/j.cveq.2018.07.009.

[26] B. Dhandayuthapani, Y. Yoshida, T. Maekawa, D.S. Kumar, Polymeric scaffolds in tissue engineering application: A review, Int. J. Polym. Sci. 2011 (2011) 1–19, http://dx.doi.org/10.1155/2011/290602.

[27] Y.S. Nam, T.G. Park, Porous biodegradable polymeric scaffolds prepared by thermally induced phase separation, J. Biomed. Mater. Res. 47 (1) (1999) 8–17, http://dx.doi.org/10.1002/(sici)1097-4636(199910)47:1<8::aid-jbm2>3.0.co;2-l.

[28] Y. Yang, J. Zhao, Y. Zhao, L. Wen, X. Yuan, Y. Fan, Formation of porous PLGA scaffolds by a combining method of thermally induced phase separation and porogen leaching, J. Appl. Polym. Sci. 109 (2) (2008) 1232–1241, http://dx.doi.org/10.1002/app.28147.

[29] A. Salerno, M. Oliviero, E.D. Maio, S. Iannace, P.A. Netti, Design of porous polymeric scaffolds by gas foaming of heterogeneous blends, J. Mater. Sci. 20 (10) (2009) 2043–2051, http://dx.doi.org/10.1007/s10856-009-3767-4.

[30] X. Wu, Y. Liu, X. Li, P. Wen, Y. Zhang, Y. Long, X. Wang, Y. Guo, F. Xing, J. Gao, Preparation of aligned porous gelatin scaffolds by unidirectional freeze-drying method, Acta Biomater. 6 (3) (2010) 1167–1177, http://dx.doi.org/10.1016/j.actbio.2009.08.041.

[31] H. Yoshimoto, Y. Shin, H. Terai, J. Vacanti, A biodegradable nanofiber scaffold by electrospinning and its potential for bone tissue engineering, Biomaterials 24 (12) (2003) 2077–2082, http://dx.doi.org/10.1016/s0142-9612(02)00635-x.

[32] F. Klein, B. Richter, T. Striebel, C.M. Franz, G. Freymann, M. Wegener, M. Bastmeyer, Two-component polymer scaffolds for controlled three-dimensional cell culture, Adv. Mater. 23 (11) (2011) 1341–1345.

[33] B. Richter, V. Hahn, S. Bertels, T.K. Claus, M. Wegener, G. Delaittre, C. Barner-Kowollik, M. Bastmeyer, Guiding cell attachment in 3D microscaffolds selectively functionalized with two distinct adhesion proteins, Adv. Mater. 29 (5) (2017).

[34] C. Maibohm, A. Saldana-Lopez, O.F. Silvestre, J.B. Nieder, 3D polymer architectures for the identification of optimal dimensions for cellular growth of 3D cellular models, Polymers 14 (19) (2022) 4168, http://dx.doi.org/10.3390/polym14194168.

[35] D. Ricci, M. Nava, T. Zandrini, G. Cerullo, M. Raimondi, R. Osellame, Scaling-up techniques for the nanofabrication of cell culture substrates via two-photon polymerization for industrial-scale expansion of stem cells, Materials 10 (1) (2017) 66, http://dx.doi.org/10.3390/ma10010066.

[36] M.M. Nava, A. Piuma, M. Figliuzzi, I. Cattaneo, B. Bonandrini, T. Zandrini, G. Cerullo, R. Osellame, A. Remuzzi, M.T. Raimondi, Two-photon polymerized “nichoid” substrates maintain function of pluripotent stem cells when expanded under feeder-free conditions, Stem Cell Res. Ther. 7 (1) (2016) 132, http://dx.doi.org/10.1186/s13287-016-0387-z.

[37] T. Weiß, G. Hildebrand, R. Schade, K. Liefeith, Two-photon polymerization for microfabrication of three-dimensional scaffolds for tissue engineering application, Eng. Life Sci. 9 (5) (2009) 384–390, http://dx.doi.org/10.1002/elsc.200900002.

[38] J. Mačiulaitis, M. Deveikytė, S. Rekštytė, M. Bratchikov, A. Darinskas, A. Šimbelytė, G. Daunoras, A. Laurinavičienė, A. Laurinavičius, R. Gudas, M. Malinauskas, R. Mačiulaitis, Preclinical study of SZ2080 material 3D microstructured scaffolds for cartilage tissue engineering made by femtosecond direct laser writing lithography, Biofabrication 7 (1) (2015) 015015, http://dx.doi.org/10.1088/1758-5090/7/1/015015.

[39] E.D. Lemma, B. Spagnolo, M.D. Vittorio, F. Pisanello, Studying cell mechanobiology in 3D: The two-photon lithography approach, Trends Biotechnol. 37 (4) (2019) 358–372, http://dx.doi.org/10.1016/j.tibtech.2018.09.008.

[40] B.N.L. Costa, R.M.R. Adão, C. Maibohm, A. Accardo, V.F. Cardoso, J.B. Nieder, Cellular interaction of bone marrow mesenchymal stem cells with polymer and hydrogel 3D microscaffold templates, ACS Appl. Mater. Interfaces 14 (11) (2022) 13013–13024, http://dx.doi.org/10.1021/acsami.1c23442.

[41] M. Diamantopoulou, N. Karathanasopoulos, D. Mohr, Stress-strain response of polymers made through two-photon lithography: Micro-scale experiments and neural network modeling, Addit. Manuf. 47 (2021) 102266, http://dx.doi.org/10.1016/j.addma.2021.102266.

[42] M.V. Santos, S.N.C. Santos, R.J. Martins, J.M.P. Almeida, K.T. Paula, G.F.B. Almeida, S.J.L. Ribeiro, C.R. Mendonça, Femtosecond direct laser writing of silk fibroin optical waveguides, J. Mater. Sci. Mater 30 (18) (2019) 16843–16848, http://dx.doi.org/10.1007/s10854-019-01406-w.

[43] D.S. Correa, P. Tayalia, G. Cosendey, D.S. dos Santos, R.F. Aroca, E. Mazur, C.R. Mendonca, Two-photon polymerization for fabricating structures containing the biopolymer chitosan, J. Nanosci. Nanotechnol. 9 (10) (2009) 5845–5849, http://dx.doi.org/10.1166/jnn.2009.1292.

[44] K. Parkatzidis, M. Chatzinikolaidou, M. Kaliva, A. Bakopoulou, M. Farsari, M. Vamvakaki, Multiphoton 3D printing of biopolymer-based hydrogels, ACS Biomater. Sci. Eng. 5 (11) (2019) 6161–6170, http://dx.doi.org/10.1021/acsbiomaterials.9b01300.

[45] L. Brigo, A. Urciuolo, S. Giulitti, G.D. Giustina, M. Tromayer, R. Liska, N. Elvassore, G. Brusatin, 3D high-resolution two-photon crosslinked hydrogel structures for biological studies, Acta Biomater. 55 (2017) 373–384, http://dx.doi.org/10.1016/j.actbio.2017.03.036.

[46] E. Ežerskytė, M. Vengris, K. Gineitis, G. Merkininkaitė, B. Leber, R. Vargalis, P. Stiegler, P. Schemmer, S. Šakirzanovas, A. Kielaitė-Gulla, K. Strupas, L. Jonušauskas, Qualitative comparison between different biopolymers for usage in two-photon polymerization towards liver regeneration, Opt. Mater. Express 12 (7) (2022) 2550, http://dx.doi.org/10.1364/ome.459057.

[47] S. Pashneh-Tala, R. Owen, H. Bahmaee, S. Rekštytė, M. Malinauskas, F. Claeyssens, Synthesis, characterization and 3D micro-structuring via 2-photon polymerization of poly(glycerol sebacate)-methacrylate - An elastomeric degradable polymer, Front. Phys. 6 (2018) 41, http://dx.doi.org/10.3389/fphy.2018.00041.

[48] C.A. Coenjarts, C.K. Ober, Two-photon three-dimensional microfabrication of poly(Dimethylsiloxane) elastomers, Chem. Mater. 16 (26) (2004) 5556–5558, http://dx.doi.org/10.1021/cm048717z.

[49] S. Rekštytė, M. Malinauskas, S. Juodkazis, Three-dimensional laser micro-sculpturing of silicone: towards bio-compatible scaffolds, Opt. Express 21 (14) (2013) 17028–17041, http://dx.doi.org/10.1364/oe.21.017028.

[50] C. Schizas, V. Melissinaki, A. Gaidukeviciute, C. Reinhardt, C. Ohrt, V. Dedoussis, B.N. Chichkov, C. Fotakis, M. Farsari, D. Karalekas, On the design and fabrication by two-photon polymerization of a readily assembled micro-valve, Int. J. Adv. Manuf. Technol. 48 (5–8) (2009) 435–441, http://dx.doi.org/10.1007/s00170-009-2320-4.

[51] P. Danilevičius, R.A. Rezende, F.D.A.S. Pereira, A. Selimis, V. Kasyanov, P.Y. Noritomi, J.V.L. da Silva, M. Chatzinikolaidou, M. Farsari, V. Mironov, Burr-like, laser-made 3D microscaffolds for tissue spheroid encagement, Biointerphases 10 (2) (2015) 021011, http://dx.doi.org/10.1116/1.4922646.

[52] O. Guillaume, O. Kopinski-Grünwald, G. Weisgrab, T. Baumgartner, A. Arslan, K. Whitmore, S. Vlierberghe, A. Ovsianikov, Hybrid spheroid microscaffolds as modular tissue units to build macro-tissue assemblies for tissue engineering, Acta Biomater. (2022) http://dx.doi.org/10.1016/j.actbio.2022.03.010.

[53] P. Danilevičius, A. Žukauskas, G. Bičkauskaitė, V. Purlys, M. Rutkauskas, T. Gertus, D. Paipulas, J. Matukaitė, D. Baltriukienė, M. Malinauskas, Laser-micro/nanofabricated 3D polymers for tissue engineering applications, Latv. J. Phys. Tech. Sci. 48 (2) (2011) 32–43, http://dx.doi.org/10.2478/v10047-011-0013-x.

[54] A. Ovsianikov, J. Viertl, B. Chichkov, M. Oubaha, B. MacCraith, I. Sakellari, A. Giakoumaki, D. Gray, M. Vamvakakian, M. Farsari, C. Fotakis, Ultra-low shrinkage hybrid photosensitive material for two-photon polymerization microfabrication, ACS Nano 2 (11) (2008) 2257–2262.

[55] M. Razavi, A.S. Thakor, An oxygen plasma treated poly(dimethylsiloxane) bioscaffold coated with polydopamine for stem cell therapy, J. Mater. Sci., Mater. Med. 29 (5) (2018) http://dx.doi.org/10.1007/s10856-018-6077-x.

[56] M. Malinauskas, A. Žukauskas, G. Bičkauskaitė, R. Gadonas, S. Juodkazis, Mechanisms of three-dimensional structuring of photo-polymers by tightly focussed femtosecond laser pulses, Opt. Express 18 (10) (2010) 10209–10221, http://dx.doi.org/10.1364/oe.18.010209.

[57] J.B. Mueller, J. Fischer, Y.J. Mange, T. Nann, M. Wegener, In-situ local temperature measurement during three-dimensional direct laser writing, Appl. Phys. Lett. 103 (12) (2013) 123107, http://dx.doi.org/10.1063/1.4821556.

[58] R. Buividas, S. Rekštytė, M. Malinauskas, S. Juodkazis, Nano-groove and 3D fabrication by controlled avalanche using femtosecond laser pulses, Opt. Mater. Express 3 (10) (2013) 1674–1686, http://dx.doi.org/10.1364/ome.3.001674.

[59] L.J. Jiang, J.H. Campbell, Y.F. Lu, T. Bernat, N. Petta, Direct writing target structures by two-photon polymerization, Fusion Sci. Technol. 70 (2) (2016) 295–309.

[60] J.S. Oakdale, R.F. Smith, J.-B. Forien, W.L. Smith, S.J. Ali, L.B. Bayu Aji, T.M. Willey, J. Ye, A.W. van Buuren, M.A. Worthington, S.T. Prisbrey, H.S. Park, P.A. Amendt, T.F. Baumann, J. Biener, Direct laser writing of low-density interdigitated foams for plasma drive shaping, Adv. Funct. Mater. 27 (43) (2017) 1702425.

[61] A. Accardo, M.-C. Blatché, R. Courson, I. Loubinoux, C. Thibault, L. Malaquin, C. Vieu, Multiphoton direct laser writing and 3D imaging of polymeric freestanding architectures for cell colonization, Small 13 (27) (2017) 1700621, http://dx.doi.org/10.1002/smll.201700621.

[62] D.J. Rosenkrantz, R.E. Stearns, P.M. Lewis, Approximate algorithms for the traveling salesperson problem, in: 15th Annual Symposium on Switching and Automata Theory, IEEE, 1974, pp. 33–42, http://dx.doi.org/10.1109/swat.1974.4.

[63] L. Jonušauskas, S. Rekštyte, M. Malinauskas, Augmentation of direct laser writing fabrication throughput for three-dimensional structures by varying focusing conditions, Opt. Eng. 53 (12) (2014) 125102, http://dx.doi.org/10.1117/1.oe.53.12.125102.

[64] A.C. Lamont, A.T. Alsharhan, R.D. Sochol, Geometric determinants of in-situ direct laser writing, Sci. Rep. 9 (1) (2019) 394, http://dx.doi.org/10.1038/s41598-018-36727-z.

[65] I.M. Handrea-Dragan, I. Botiz, A.-S. Tatar, S. Boca, Patterning at the micro/nano-scale: Polymeric scaffolds for medical diagnostic and cell-surface interaction applications, Colloids Surf. B 218 (2022) 112730, http://dx.doi.org/10.1016/j.colsurfb.2022.112730.

[66] G.R.B.E. Romer, P. Bechtold, Electro-optic and acousto-optic laser beam scanners, Phys. Procedia 56 (2014) 29–39, http://dx.doi.org/10.1016/j.phpro.2014.08.092.

[67] A.K. Nguyen, S.D. Gittard, A. Koroleva, S. Schlie, A. Gaidukeviciute, B.N. Chichkov, R.J. Narayan, Two-photon polymerization of polyethylene glycol diacrylate scaffolds with riboflavin and triethanolamine used as a water-soluble photoinitiator, Regen. Med. 8 (6) (2013) 725–738, http://dx.doi.org/10.2217/rme.13.60.

[68] M. Tromayer, A. Dobos, P. Gruber, A. Ajami, R. Dedic, A. Ovsianikov, R. Liska, A biocompatible diazosulfonate initiator for direct encapsulation of human stem cells via two-photon polymerization, Polym. Chem. 9 (22) (2018) 3108–3117, http://dx.doi.org/10.1039/c8py00278a.

[69] C.-C. Wang, J.-Y. Chen, J. Wang, The selection of photoinitiators for photopolymerization of biodegradable polymers and its application in digital light processing additive manufacturing, J. Biomed. Mater. Res. Part A 110 (1) (2021) 204–216, http://dx.doi.org/10.1002/jbm.a.37277.

[70] R. Liu, Y. Lin, F. Hu, R. Liu, T. Ruan, G. Jiang, Observation of emerging photoinitiator additives in household environment and sewage sludge in China, Environ. Sci. Technol. 50 (1) (2015) 97–104, http://dx.doi.org/10.1021/acs.est.5b04977.

[71] A.-V. Do, K.S. Worthington, B.A. Tucker, A.K. Salem, Controlled drug delivery from 3D printed two-photon polymerized poly(ethylene glycol) dimethacrylate devices, Int. J. Pharm. 552 (1–2) (2018) 217–224, http://dx.doi.org/10.1016/j.ijpharm.2018.09.065.

[72] M. Dudziak, I. Topolniak, D. Silbernagl, K. Altmann, H. Sturm, Long-time behavior of surface properties of microstructures fabricated by multiphoton lithography, Nanomaterials 11 (12) (2021) 3285, http://dx.doi.org/10.3390/nano11123285.

[73] P. Abnave, E. Ghigo, Role of the immune system in regeneration and its dynamic interplay with adult stem cells, Semin. Cell Dev. Biol. 87 (2019) 160–168, http://dx.doi.org/10.1016/j.semcdb.2018.04.002.

[74] P. DanilevičIus, S. Rekštytė, E. BalčIūnas, A. Kraniauskas, R. Širmenis, D. Baltriukienė, M. Malinauskas, V. Bukelskienė, R. Gadonas, V. Sirvydis, A. Piskarskas, Direct laser fabrication of polymeric implants for cardiovascular surgery, Mater. Sci. 18 (2) (2012) http://dx.doi.org/10.5755/j01.ms.18.2.1917.

[75] A. Dobos, J. Hoorick, W. Steiger, P. Gruber, M. Markovic, O.G. Andriotis, A. Rohatschek, P. Dubruel, P.J. Thurner, S. Vlierberghe, S. Baudis, A. Ovsianikov, Thiol–gelatin–norbornene bioink for laser-based high-definition bioprinting, Adv. Healthc. Mater. 9 (15) (2019) 1900752, http://dx.doi.org/10.1002/adhm.201900752.

[76] MPO 100 setup datasheet, Multiphoton optics Ghmb, 2022. (Accessed August 2022).

[77] A. Žemaitis, M. Gaidys, P. Gečys, G. Račiukaitis, M. Gedvilas, Rapid high-quality 3D micro-machining by optimised efficient ultrashort laser ablation, Opt. Lasers Eng. 114 (2018) 83–89, http://dx.doi.org/10.1016/j.optlaseng.2018.11.001.

[78] A. Žemaitis, P. Gečys, M. Barkauskas, G. Račiukaitis, M. Gedvilas, Highly-efficient laser ablation of copper by bursts of ultrashort tuneable (fs-ps) pulses, Sci. Rep. 9 (1) (2019) 12280, http://dx.doi.org/10.1038/s41598-019-48779-w.

[79] D. Čereška, A. Žemaitis, G. Kontenis, G. Nemickas, L. Jonušauskas, On-demand wettability via combining fs laser surface structuring and thermal post-treatment, Materials 15 (6) (2022) 2141, http://dx.doi.org/10.3390/ma15062141.

[80] D. Andrijec, D. Andriukaitis, R. Vargalis, T. Baravykas, T. Drevinskas, O. Kornyšova, A. Butkuė, V. Kaškonienė, M. Stankevičius, H. Gricius, A. Jagelavičius, A. Maruška, L. Jonušauskas, Hybrid additive-subtractive femtosecond 3D manufacturing of nanofilter-based microfluidic separator, Appl. Phys. A 127 (10) (2021) http://dx.doi.org/10.1007/s00339-021-04872-4.

[81] D. Yang, L. Liu, Q. Gong, Y. Li, Rapid two-photon polymerization of an arbitrary 3D microstructure with 3D focal field engineering, Macromol. Rapid Commun. 40 (8) (2019) 1900041, http://dx.doi.org/10.1002/marc.201900041.

[82] G. Kontenis, D. Gailevičius, L. Jonušauskas, V. Purlys, Dynamic aberration correction via spatial light modulator (SLM) for femtosecond direct laser writing: towards spherical voxels, Opt. Express 28 (19) (2020) 27850–27864, http://dx.doi.org/10.1364/oe.397006.

[83] V. Hahn, P. Kiefer, T. Frenzel, J. Qu, E. Blasco, C. Barner-Kowollik, M. Wegener, Rapid assembly of small materials building blocks (Voxels) into large functional 3D metamaterials, Adv. Funct. Mater. 30 (26) (2020) 1907795, http://dx.doi.org/10.1002/adfm.201907795.

[84] C. Maibohm, O.F. Silvestre, J. Borme, M. Sinou, K. Heggarty, J.B. Nieder, Multi-beam two-photon polymerization for fast large area 3D periodic structure fabrication for bioapplications, Sci. Rep. 10 (1) (2020) http://dx.doi.org/10.1038/s41598-020-64955-9.

[85] J. Park, B.G. Jeong, S.I. Kim, D. Lee, J. Kim, C. Shin, C.B. Lee, T. Otsuka, J. Kyoung, S. Kim, K.-Y. Yang, Y.-Y. Park, J. Lee, I. Hwang, J. Jang, S.H. Song, M.L. Brongersma, K. Ha, S.-W. Hwang, H. Choo, B.L. Choi, All-solid-state spatial light modulator with independent phase and amplitude control for three-dimensional LiDAR applications, Nat. Nanotechnol. 16 (1) (2020) 69–76, http://dx.doi.org/10.1038/s41565-020-00787-y.

[86] B. Zeng, Z. Huang, A. Singh, Y. Yao, A.K. Azad, A.D. Mohite, A.J. Taylor, D.R. Smith, H.-T. Chen, Hybrid graphene metasurfaces for high-speed mid-infrared light modulation and single-pixel imaging, Light Sci. Appl. 7 (1) (2018) http://dx.doi.org/10.1038/s41377-018-0055-4.

[87] Y. Xie, M. Praeger, J.A. Grant-Jacob, R.W. Eason, B. Mills, Motion control for laser machining via reinforcement learning, Opt. Express 30 (12) (2022) 20963, http://dx.doi.org/10.1364/oe.454793.

[88] G.K. Sarkon, B. Safaei, M.S. Kenevisi, S. Arman, Q. Zeeshan, State-of-the-art review of machine learning applications in additive manufacturing from; Design to manufacturing and property control, Arch. Comput. Methods Eng. (2022) http://dx.doi.org/10.1007/s11831-022-09786-9.

[89] C. BenMessaoud, H. Kharrazi, K.F. MacDorman, Facilitators and barriers to adopting robotic-assisted surgery: Contextualizing the unified theory of acceptance and use of technology, PLoS One 6 (1) (2011) e16395, http://dx.doi.org/10.1371/journal.pone.0016395.

[90] C. Christodoulakis, A. Asgarian, S. Easterbrook, Barriers to adoption of information technology in healthcare, in: CASCON '17: Proceedings of the 27th Annual International Conference on Computer Science and Software Engineering, 2017, pp. 66–75.

[91] C.-Y. Liaw, M. Guvendiren, Current and emerging applications of 3D printing in medicine, Biofabrication 9 (2) (2017) 024102, http://dx.doi.org/10.1088/1758-5090/aa7279.

[92] V.M. Vaz, L. Kumar, 3D printing as a promising tool in personalized medicine, AAPS PharmSciTech 22 (1) (2021) 49, http://dx.doi.org/10.1208/s12249-020-01905-8.

[93] M. Salmi, Additive manufacturing processes in medical applications, Materials 14 (1) (2021) 191, http://dx.doi.org/10.3390/ma14010191.